tvst

Article

Multimodal Retinal Imaging and Microperimetry Reveal a Novel Phenotype and Potential Trial End Points in *CRB1*-Associated Retinopathies

Danial Roshandel[1], Jennifer A. Thompson[2], Rachael C. Heath Jeffery[1,6], Danuta M. Sampson[1,3], Enid Chelva[2], Terri L. McLaren[1,2], Tina M. Lamey[1,2], John N. De Roach[1,2], Shane R. Durkin[4,5], and Fred K. Chen[1,6,7]

[1] Centre for Ophthalmology and Visual Science (incorporating Lions Eye Institute), The University of Western Australia, Australia
[2] Australian Inherited Retinal Disease Registry and DNA Bank, Department of Medical Technology and Physics, Sir Charles Gairdner Hospital, Perth, Western Australia, Australia
[3] Surrey Biophotonics, Centre for Vision, Speech and Signal Processing and School of Biosciences and Medicine, The University of Surrey, Guildford, UK
[4] Discipline of Ophthalmology and Visual Science, The University of Adelaide, South Australia, Australia
[5] Department of Ophthalmology, The Royal Adelaide and Queen Elizabeth Hospital, Adelaide, South Australia, Australia
[6] Department of Ophthalmology, Royal Perth Hospital, Perth, Western Australia, Australia
[7] Department of Ophthalmology, Perth Children's Hospital, Nedlands, Western Australia, Australia

Correspondence: Fred K. Chen, Lions Eye Institute, 2 Verdun Street, Nedlands WA, Australia. e-mail: fredchen@lei.org.au

Received: October 29, 2020
Accepted: January 20, 2021
Published: February 25, 2021

Keywords: crumbs cell polarity complex component 1 (*CRB1*); multimodal imaging; retinitis pigmentosa; macular dystrophy; natural history

Citation: Roshandel D, Thompson JA, Heath Jeffery RC, Sampson DM, Chelva E, McLaren TL, Lamey TM, De Roach JN, Durkin SR, Chen FK. Multimodal retinal imaging and microperimetry reveal a novel phenotype and potential trial end points in *CRB1*-associated retinopathies. Trans Vis Sci Tech. 2021;10(2):38, https://doi.org/10.1167/tvst.10.2.38

Purpose: Biallelic crumbs cell polarity complex component 1 (*CRB1*) mutations can present as Leber congenital amaurosis (LCA), retinitis pigmentosa (RP), or cystic maculopathy. This study reports a novel phenotype of asymptomatic fenestrated slit maculopathy (AFSM) and examines macular volume profile and microperimetry as clinical trial end points in *CRB1*-associated retinopathies.

Methods: Twelve patients from nine families with *CRB1* mutation were recruited. Ultra-widefield (UWF) color fundus photography and autofluorescence (AF), spectral-domain optical coherence tomography (SD-OCT), microperimetry, and adaptive optics (AO) imaging were performed. Macular volume profiles were compared with age-matched healthy controls. Genotyping was performed using APEX genotyping microarrays, targeted next-generation sequencing, and Sanger sequencing.

Results: We identified one patient with LCA, five patients with RP, and four patients with macular dystrophy (MD) with biallelic *CRB1* mutations. Two siblings with compound heterozygote genotype (c.[2843G>A]; [498_506del]) had AFSM characterized by localized outer retinal disruption on SD-OCT and parafoveal cone loss on AO imaging despite normal fundus appearance, visual acuity, and foveal sensitivity. UWF AF demonstrated preserved para-arteriolar retinal pigment epithelium (PPRPE) in all patients with RP. Microperimetry documented preserved central retinal function in six patients. The ratio of perifoveal-to-foveal retinal volume was greater than controls in 89% (8/9) of patients with RP or MD, whereas central subfield and total macular volume were outside normal limits in 67% (6/9).

Conclusions: AO imaging was helpful in detecting parafoveal cone loss in asymptomatic patients. Macular volume profile and microperimetry parameters may have utility as *CRB1* trials end points.

Translational Relevance: Macular volume and sensitivity can be used as structural and functional end points for trials on *CRB1*-associated RP and MD.

Introduction

Crumbs cell polarity complex component 1 (*CRB1*; OMIM: #604210) is a transmembrane protein, located within the subapical region of human photoreceptors that plays a critical role in retinal development, structure, and function.[1,2] Biallelic mutations in *CRB1* have been implicated in 3% to 9% of autosomal recessive retinitis pigmentosa (arRP), including retinitis pigmentosa 12 (RP12; OMIM: #600105)[3] and 7% to 17% of Leber congenital amaurosis (LCA), also known as LCA8 (OMIM: #613835).[4,5] Maculopathy with or without foveal schisis is a more recently recognized phenotype associated with *CRB1* mutations.[6–11] Given gene therapy for *CRB1*-associated retinopathy is already underway in an animal model,[12] it is timely to examine the various imaging biomarkers that could be considered in future *CRB1* treatment trials.

CRB1-associated retinitis pigmentosa (*CRB1*-RP) has been associated with coarse retinal lamination, thick retina, preserved para-arteriolar retinal pigment epithelium (PPRPE), hypermetropia, cystoid macular edema (CMO), and retinal telangiectasia with Coat's-like reaction.[13] For example, the likelihood of detecting *CRB1* mutation in patients with RP is higher among those presenting with PPRPE (66%–74%) or retinal telangiectasia (31%–53%).[4] Jacobson and colleagues reported abnormal parafoveal retinal thickening in eight patients with *CRB1*-associated LCA or early-onset severe RP.[14] Their study used low resolution time-domain optical coherence tomography (OCT) cross section images without thickness mapping and only a relatively small number of healthy control subjects were recruited ($n = 3$). In a cohort of 55 patients with *CRB1*-RP, Talib et al. reported perifoveal retinal thickening in 82% (9/11) of patients and PPRPE in 26% (13/50) and 33% (3/9) of patients on widefield color composite fundus photographs and fundus autofluorescence (FAF) imaging, respectively.[15] Although these cases were followed for 15.4 years, adaptive optics (AO) imaging and microperimetry data were not presented. Whereas universal functional markers, such as full-field stimulus and pupillography, may be used as trial end point in patients with late-stage RP caused by *CRB1* mutations,[16] they may not be useful in patients with early-stage RP or maculopathy. Hence, more localized functional tests are required for monitoring disease progression in patients with the latter manifestation of *CRB1*, which is gaining recognition as an important differential diagnosis of inherited isolated cystic maculopathy. *CRB1*-associated maculopathy is typically associated with a 9-bp deletion in exon 2,[9–11] with few exceptions.[7,8] Unlike *CRB1*-RP, patients with maculopathy can be myopic[8] and have a well-developed retinal structure.[7] The hallmark of *CRB1*-maculopathy in OCT is early-onset schitic/cystoid maculopathy, which resolves during several years to decades leading to severe macular atrophy.[10,11] However, none of the previous studies quantified the retinal sensitivity and macular volume parameters. In addition, there has been no report of a patient with biallelic *CRB1* mutation with normal visual acuity and no apparent macular architectural change.

In the present study, we use multimodal retinal imaging and microperimetry to characterize structural and functional changes in *CRB1*-associated LCA, RP, and maculopathy. In addition, we describe a previously unreported phenotype of asymptomatic fenestrated slit maculopathy.

Patients and Methods

Subjects

The participants in this case series were enrolled as part of the Western Australia Retinal Degeneration (WARD) Study. Genetic diagnosis was established through the Australian Inherited Retinal Disease Registry and DNA Bank. The study protocol adhered to the tenets of the Declaration of Helsinki and ethics approval was obtained from the Human Ethics Committee of the Office of Research Enterprise, The University of Western Australia (RA/4/1/7916), and Sir Charles Gairdner Hospital Human Research Ethics Committee (approval number 2001–053). Written informed consent was obtained from the participants prior to inclusion in the study.

Study Protocol and Clinical Assessment

Diagnosis of inherited retinal disease (IRD) was confirmed by an experienced retinal specialist (author F.K.C.) based on history and clinical examination and/or electroretinography (ERG). Clinical assessment involved obtaining a full medical and ocular history, best-corrected visual acuity (BCVA), and dilated fundus examination. ERG (RETIport version 3.2; Roland Consult, Brandenburg, Germany, or in-house custom built) was recorded in accordance with International Society for Clinical Electrophysiology of Vision (ISCEV) standards.[17] Assessment of visual fields was

undertaken using fundus-controlled microperimetry (Macular Integrity Assessment [MAIA] perimeter; CenterVue, Padova, Italy). The large 10-2 (68 test loci) and the small radial (37 test loci, 37R) grid patterns were used to map the retinal sensitivity profile within the macular (central 20 degrees field) and foveal (central 6 degrees field) regions, respectively (Supplementary Figs. S1A, S1B).

Detailed multimodal imaging was performed in all cases, including widefield color fundus photography and green-light fundus autofluorescence (California; Optos plc., Dunfermline, UK) and spectral domain optical coherence tomography (SD-OCT, Spectralis; Heidelberg Engineering, Heidelberg, Germany). Fovea-centered macular volume scans were performed in a 30 degrees × 25 degrees area covering the early treatment diabetic retinopathy study (ETDRS) 1, 3, and 6 mm grid pattern (Supplementary Fig. S1C). Volume scans consisted of 61 horizontal B-scans separated by approximately 130 µm between each scan. Inner limiting membrane and Bruch's membrane were segmented automatically using the manufacturer software (HEYEX version 1.9.14.0; Heidelberg Engineering) and adjusted manually by a trained ophthalmologist (author D.R.) in cases with segmentation error. A dense raster 15 degrees × 10 degrees volume scan (97 slices, 30 µm intervals) was performed in cases with central residual island of vision to visualize the en face reflectance map of the interdigitating zone (IZ). Autofluorescence (AF) imaging was performed using a scanning laser ophthalmoscope (Spectralis HRA2; Heidelberg Engineering) with short-wavelength AF (SW-AF; λ = 488 nm) and near-infrared AF (NI-AF; λ = 787 nm) modalities. Flood-illumination AO retinal imaging using rtx1 AO camera (Imagine Eyes, Orsay, France) was performed in selected patients (n = 3) with fixation ability and without cataract and CMO. Multiple overlapping 4 degrees × 4 degrees images covering the central 6 degrees were taken at the photoreceptor level. Individual tiles were stitched together using i2k Retina software (DualAlign LLC, Clifton Park, NY, USA) and overlayed on high-resolution IR + OCT image. The location of the fovea was marked on the montaged AO image of each eye.

To compare SD-OCT macular volume measurements in a normal population, 80 control subjects were grouped into three age categories: 20 to 40 years (n = 19), 41 to 60 years (n = 36), and 61 to 75 years (n = 25). Mean and standard deviations of macular volume indices were calculated for each age subgroup (Supplementary Table S1).

Outcome Measures

BCVA was measured using the ETDRS chart and recorded as ETDRS letter score and converted to Snellen equivalents. Microperimetry point-wise sensitivity (PWS) was classified into normal sensitivity (≥25 dB), relative scotoma (0–24 dB), or absolute scotoma (<0 dB). Mean retinal sensitivity (MS), number of scotomatous loci and number of seeing loci (sensitivity ≥0 dB) were reported for both the small radial and 10-2 grids.

The ETDRS grid (6 mm diameter) central subfield volume (CSV; 1 mm diameter), total macular volume (TMV), and average volume of the inner and outer ETDRS rings at four quadrants were recorded for each OCT volume scan. In addition, ratio of the TMV, outer ring volume (ORV) and inner ring volume (IRV) to CSV were calculated. AO images were analyzed using AODetect version 3.0 (Imagine Eyes). Cone density (CD) was measured at 2 degrees, 3 degrees, and 4 degrees along 4 meridional directions (Supplementary Fig. S1D) and angular values (cell/deg^2) were reported. Patients' CD values were compared with normal rtx1 ranges (average ± 2 SD) reported by Legras and colleagues.[18] In addition, previously validated custom software[19] was used for semi-automated segmentation of AO montages to create a parafoveal cone density map.

Genotyping and Pathogenicity Assessment

Genomic DNA samples were collected, processed, and stored as previously described.[20] Genomic DNA was analyzed using the APEX ARRP microarray (Asper Biotech, Estonia), bidirectional Sanger sequencing (Macrogen, Seoul, South Korea, or Asper Biotech), or various next-generation sequencing (NGS) panels,[21] and confirmed by Sanger sequencing (Casey Eye Institute, CEI Molecular Diagnostics Laboratory, Portland, OR, USA, or Molecular Vision Laboratory, Hillsboro, OR, USA). Cascade testing of family members was analyzed by Sanger sequencing, performed at CEI, the Australian Genome Research Facility (AGRF; Perth, WA, Australia), or at the Lions Eye Institute (Supplementary Table S2).

Variants are described in accordance with Human Genome Variation Society recommendations.[22] Pathogenicity was assessed using M-CAP,[23] REVEL,[24] Mutation Taster,[25] PolyPhen2,[26] SIFT, SIFT Indel,[27] VEST Indel,[28] and the Alamut Visual Splicing Suite, with information sought from LOVD, ClinVar, dbSNP, HGMD,[29] Exome Sequencing Project, and gnomAD.[30] Pathogenicity was interpreted in accordance with

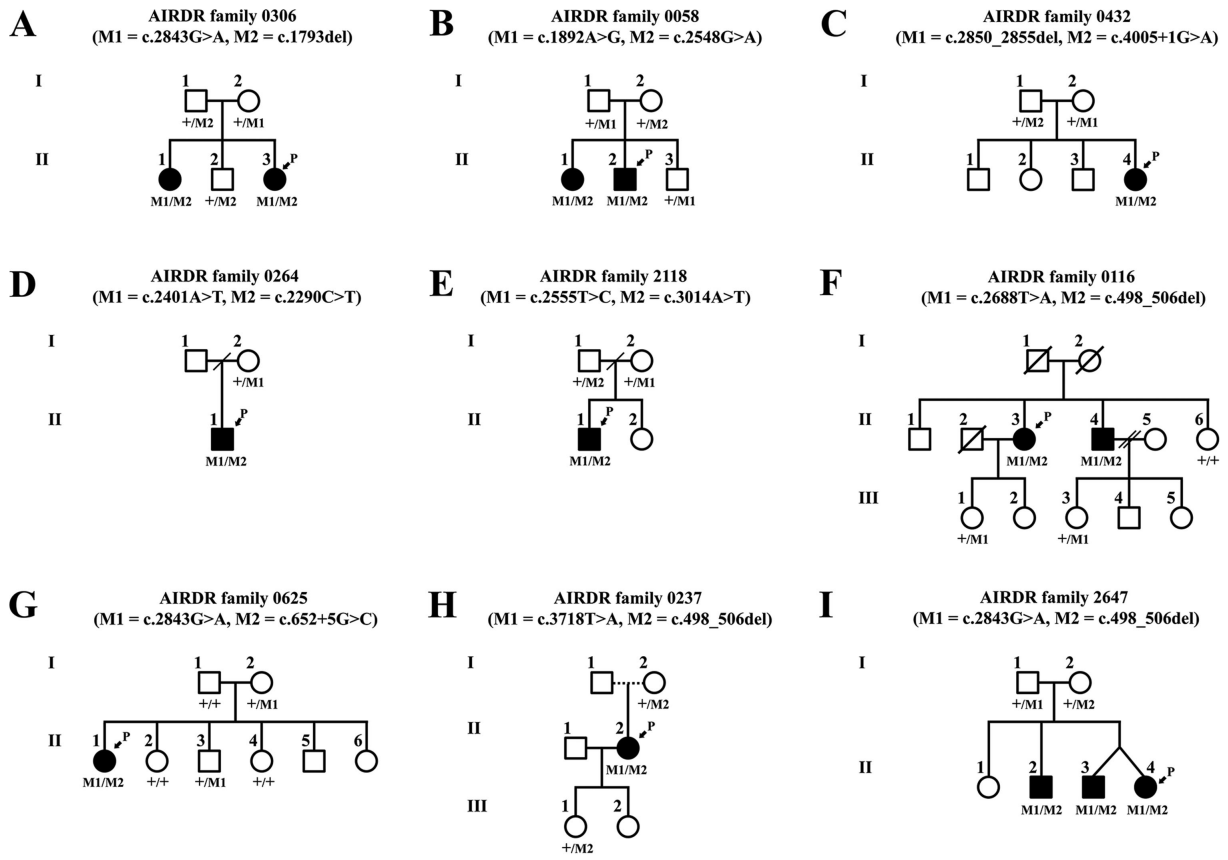

Figure 1. Pedigrees of families with *CRB1*-associated Leber congenital amaurosis (**A**), retinitis pigmentosa (**B–E**), and maculopathy (**F–I**). A novel phenotype (asymptomatic fenestrated slit maculopathy) was observed in two siblings (II:2 and II:4) of family 2647 **I**, whereas the other sibling (II:3) had typical macular dystrophy.

current guidelines proposed by the American College of Medical Genetics and Genomics and the Association for Molecular Pathology,[31] and associated literature.[32,33]

Statistical Analysis

Data were recorded in Statistical Package for the Social Sciences (SPSS) version 23 (SPSS/IBM, Inc., Chicago, IL, USA) and appropriate statistics applied after testing for normality. Quantitative data are presented as the mean (SD, range) and categorical data are presented as absolute numbers (%). For the macular volume parameters, the average and SD of the age-matched healthy subjects were calculated and values above or below 2 SD were considered significant. Z-scores of the patients' macular volume measurements were calculated as ([patient value − normal average]/SD). Rates of annual change in macular volume parameters were calculated using linear regression analysis and beta estimates were reported. Only right eye data were included in all statistical analyses.

Results

Patients

Twelve patients (5 male patients and 7 female patients) from nine Caucasian Australian families were recruited (Fig. 1). Patients were denoted by pedigree number and generation:individual. Mean age (SD, range) at baseline examination was 35 (16, 11–68) years. The mean (SD, range) age at onset of symptoms was 9 (7, 0–21) years. Demographics, clinical characteristics, and genotype are summarized in Table 1.

Spectrum of Phenotypes

Based on the pattern of retinal involvement on ultra-widefield FAF, patients were categorized into two groups, namely pan-retinopathy or maculopathy. Pan-retinopathy was further categorized into LCA and RP according to the age of onset and ocular findings. Maculopathy was categorized into macular dystrophy

Table 1. Demographics, Baseline Clinical Characteristics, and Genotypes of 12 Patients With *CRB1*-Associated Retinopathy

					BCVA		MRSE (D)		Axial length (mm)		Lens				
Pedigree ID	Subject ID	Gender	Onset, y	Age, Y	RE	LE	RE	LE	RE	LE	RE	LE	Allele 1	Allele 2	Phenotype
0306	II:3	Female	Birth[a]	28	CF	CF	−0.50	−1.00	–	–	CC	CC	c.2843G>A	c.1793del	LCA
0058	II:1	Female	21[b]	47	PL	PL	−2.25	−2.00	22.1	22.1	PSC	PSC	c.1892A>G	c.2548G>A	RP
	II:2	Male	18[b]	45	PL	PL	+0.50	−0.50	23.4	23.4	IOL	IOL			
0432	II:4	Female	8[c]	48	20/200	20/250	+4.00	+3.50	21.6	21.5	NSC	NSC	c.4005+1G>A	c.2850_2855del	
0264	II:1	Male	Birth[d]	29	20/80	20/250	+4.00	+6.75	–	–	Clear	PSC	c.2401A>T	c.2290C>T	
2118	II:1	Male	5[c]	11	20/40	20/32	+5.50	+5.00	20.0	20.1	Clear	Clear	c.2555T>C	c.3014A>T	
0116	II:3	Female	8[e]	68	HM	HM	−0.50	−0.25	21.9	22.1	IOL	IOL	c.2688T>A	c.498_506del	MD
0625	II:1	Female	10[e]	47	20/125	CF	−0.50	−0.50	22.5	22.6	Clear	NSC	c.2843G>A	c.652+5G>C	
0237	II:2	Female	11[f]	30	20/40	20/63	−1.00	−0.75	–	–	NSC	NSC	c.3718T>A	c.498_506del	
2647	II:3	Male	22[f]	23	20/40	20/250	−2.00	−2.50	24.2	24.4	Clear	Clear	c.2843G>A	c.498_506del	
	II:2	Male	NA[g]	26	20/20	20/16	−2.50	−3.00	25.7	25.6	Clear	Clear	c.2843G>A	c.498_506del	AFSM
	II:4	Female	NA[g]	23	20/20	20/20	−0.25	0.00	24.3	24.3	Clear	Clear			

[a]Nystagmus and poor visuo-motor responses shortly after birth.
[b]Visual field constriction and deterioration of visual acuity.
[c]Nyctalopia and low vision.
[d]Life-long impaired vision in the dark.
[e]Central visual loss.
[f]Blurred vision in one eye.
[g]Asymptomatic.

AFSM, asymptomatic fenestrated slit maculopathy; BCVA, best-corrected visual acuity; CC, cortical cataract; CF, counting fingers; D, diopter; EC, early childhood; HM, hand motion; IOL, intraocular lens; LCA, Lebers congenital amaurosis; LE, left eye; MD, macular dystrophy; MRSE, manifest refraction spherical equivalent; NA, not applicable; NSC, nuclear sclerosing cataract; PL, perception of light; PSC, posterior subcapsular cataract; RE, right eye; RP, retinitis pigmentosa.

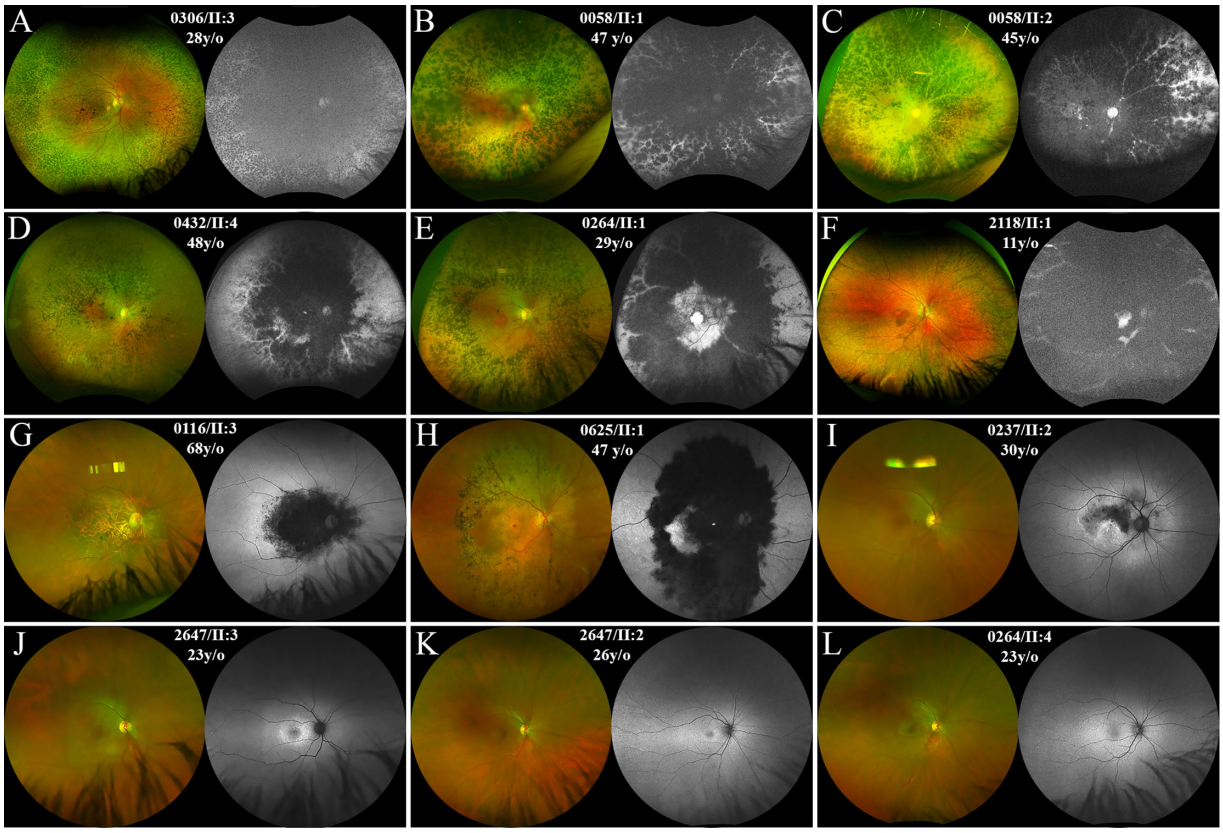

Figure 2. Ultra-widefield color fundus photograph and autofluorescence (AF) imaging show diffuse nummular pigmentation and complete loss of normal AF in patient with Leber congenital amaurosis (**A**) and midperipheral bone-spicule pigmentation and hypo-autofluorescence with central preservation of retinal pigment epithelium in patients with retinitis pigmentosa (RP) phenotype (**B–F**). Note that preserved para-arteriolar RPE (PPRPE) is best visualized in AF imaging in all patients with RP **B** to **F**. Maculopathy presented with extensive macular atrophy incorporating the optic disc (**G, H**) with some residual temporal macular autofluorescence **H**, or localized superotemporal hypo-autofluorescence surrounded by hyperautofluorescent area (**I**), or normal fundus appearance and a macular hyperautofluorescent ring in AF (**J**) in patients with macular dystrophy, or unremarkable fundus and AF in two patients with asymptomatic fenestrated slit maculopathy (**K, L**). Mild loss of normal macular hyperautofluorescence and incomplete hyperautofluorescent ring may be noted in patient 2647/II:2 **K**. Note that patients 2647/II:3 **J** and 2647/II:4 **L** are di-zygotic twins with different presentations.

(MD) and asymptomatic fenestrated slit maculopathy (AFSM) based on symptoms and multimodal imaging findings. Using this classification, we had one patient with LCA, five patients with RP, four patients with MD, and two patients with AFSM (Fig. 2). Of note, patients 2647/II:3 and II:4 who were diagnosed with MD and AFSM, respectively, were di-zygotic twins.

Central Retinal Function in Symptomatic Patients

Foveal and/or macular function was evaluated using microperimetry in 6 out of 10 symptomatic patients with severe outer retinal atrophy (3 RP and 3 MD). Serial microperimetry was available in 2 patients with RP (0432/II:4 and 2118/II:1) and 2 patients with MD (0625/II:1 and 0237/II:2; Fig. 3). Patient 0432/II:4, 48 years old, with RP, responded to 25/37 foveal stimuli and the foveal MS was 6.5 dB, whereas her BCVA was 20/250 (see Fig. 3A). After 4 years, the number of foveal seeing loci and foveal MS reduced to 20/37 loci and 4.9 dB, respectively (see Fig. 3C). The foveal sensitivity and number of seeing loci were 12.2 dB and 32/37, respectively, in the 29 year old patient with RP (see Fig. 3E). Patient 2118/II:1, 11 years old with RP, had a baseline macular seeing loci count and MS of 31 and 4.6 dB, respectively (see Fig. 3F). Follow-up examinations revealed persistent improvement in macular sensitivity over a 3-year period (see Figs. 3G, 3H). Patient 0625/II:1 with advanced MD (47 years old) had a BCVA of 20/125 in her better eye

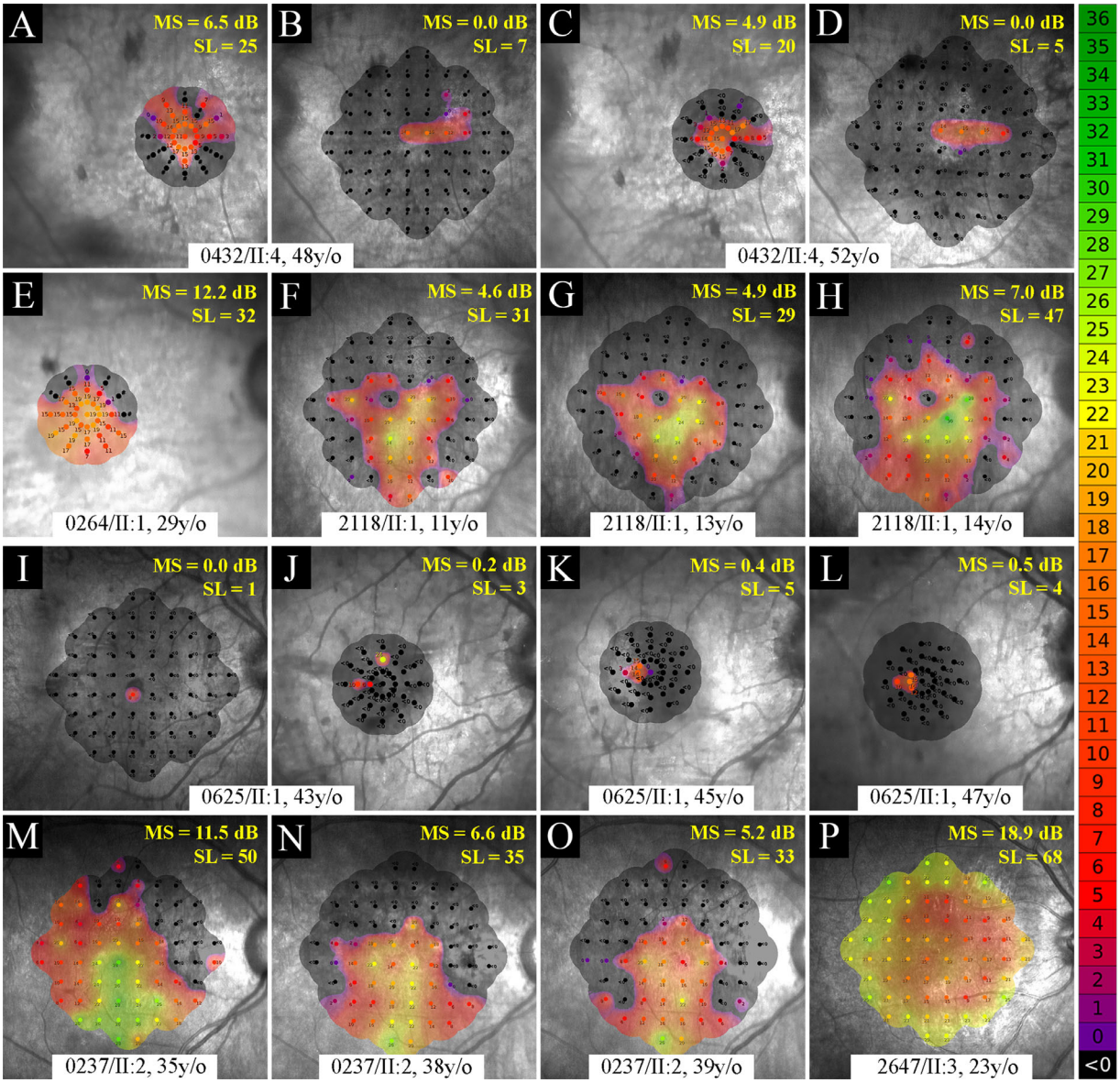

Figure 3. Microperimetry showed residual foveal and/or macular function in patients with retinitis pigmentosa (RP) (**A–H**) and macular dystrophy (MD) (**I–P**). Central retinal function was recorded despite very low visual acuity (20/250) in the left eye of a 48 year old patient with advanced RP at baseline **A** and **B**, which declined after 4 years **C** and **D**. The 29 year old patient with RP showed greater foveal MS and number of seeing loci **E**. A fairly good baseline macular sensitivity with persistent improvement during a 3-year period was observed in the 11 year old patient with RP **F** to **H**. The 43 year old patient with advanced MD who presented with extensive macular atrophy responded only to stimuli presented at the central 2 degrees (**I–J**). Follow-up examinations showed stable function over a 4-year period (**K–L**). Patient 0237/II:2 presented with localized superotemporal scotoma in 10-2 test corresponding to the atrophic area, which progressed over 4 years of follow-up (**M–O**). The youngest patient with MD responded to all 68 presented 10-2 test loci with mild central depression (**P**). MS, mean sensitivity; SL, number of seeing loci. Color coding of threshold values is shown on the right side.

(right eye) and could see only 3 stimuli on foveal grid with a mean sensitivity of 0.2 dB at baseline, which remained stable after 4 years (see Figs. 3J–L). An unusual microperimetry pattern was observed in patient 0237/II:2 characterized by a localized superotemporal scotoma on the 10-2 grid. Follow-up examination after 3 and 4 years showed enlargement of the scotoma and significant decrease in macular MS (Figs. 3M–O).

Only two patients with MD underwent ERG testing where patient 0237/II:2 showed a normal rod and subnormal cone response in full-field ERG and patient 2647/II:3 had features on multifocal and pattern ERG suggestive of macular dysfunction.

Fundus Autofluorescence and SD-OCT in Symptomatic Patients

Ultra-widefield AF showed diffuse hypo-autofluorescence in patients with pan-retinopathy and highlighted PPRPE and a variable-sized central island of preserved retinal pigment epithelium (RPE) in all patients with RP phenotype, regardless of age and disease severity (see Figs. 2B–F and Supplementary Figs. S2A–E). SD-OCT over the PPRPE showed remnants of outer retinal and RPE structures blocking choroidal transmission of light (Supplementary Fig. S2F). Patients with MD revealed either extensive macular hypo-autofluorescence incorporating the optic disc in patients 0116/II:3 (68 years old) and 0625/II:1 (47 years old), localized superotemporal hypo-autofluorescence in patient 0237/II:2 (30 years old) or macular hyperautofluorescent ring in patient 2647/II:3 (23 years old; Figs. 2G–J).

Macular SD-OCT showed coarse retinal lamination in patients with RP and diffuse outer retinal atrophy in all patients (Supplementary Fig. S3). Although remnants of photoreceptor layer were detected in all patients, an EZ line was visible only in 1 patient with RP and 3 patients with MD (Supplementary Figs. S3E, S3H, S3I, S3J). Bilateral cystoid maculopathy was observed in baseline OCT of patient 0237/II:2 and retrospective OCTs of patient 2647/II:3. Serial macular OCT revealed resolution of cystoid spaces and progressive outer retinal atrophy in both patients (Fig. 4). In addition, mild cystoid change was detected in three patients with RP phenotype (Supplementary Figs. S3B, S3C, S3F).

Macular Volume Profile

Baseline macular volume scan was available for 11 patients. None of the patients (including those with CMO in retrospective OCT scans) had cystoid maculopathy at the time of baseline imaging for the macular volume study and during follow-up phase. CSV was significantly lower than age-matched healthy controls in three of five patients with RP and three of four patients with MD, whereas TMV and ORV were significantly higher in four of five patients with RP and lower in two of four patients with MD. The ratio of TMV/CSV and ORV/CSV was higher than control group in four of five patients with RP and four of four patients with MD (8/9 symptomatic patients), with greater Z-scores for ORV/CSV (Table 2). All macular volume parameters were within normal ranges in the two patients with AFSM (see Table 2).

Longitudinal macular volume data were available in 10 patients (8 symptomatic and 2 asymptomatic) with a mean (SD, range) follow-up duration of 3.7 (1.9, 1.2–7.2) years. CSV declined at a rate of 0.002 to 0.004 mm^3 per year in 5 patients (3 RP and 2 MD) aged 35 years or above and increased at a rate of 0.003 to 0.006 mm^3 per year in 3 patients (2 RP and 1 MD) aged below 30 years. Conversely, TMV/CSV, IRV/CSV, and ORV/CSV increased in patients aged 35 years and above and declined in symptomatic patients aged below 30 years. This age-dependent pattern was not detected in TMV, IRV, and ORV change (Supplementary Table S3). Plotting volume measurements against age highlighted this age-dependent pattern, which was more prominent for TMV/CSV (Figs. 5A–C). Longitudinal change in OCT B-scan and macular volume profile in a 48 year old patient with RP with more than 7 years follow-up is shown in Figures 5D and 5E. Interestingly, despite significant decline in both CSV and TMV with increasing age, TMV/CSV ratio showed a significant increase (see Fig. 5, Supplementary Table S3).

Multimodal Imaging in AFSM

Both patients with AFSM had normal BCVA, fundus appearance, and foveal sensitivity (Figs. 6A, 6F). However, NI-AF imaging revealed a horizontal linear hypo-autofluorescence marking (Figs. 6C, 6H) and corresponding attenuation of the subfoveal EZ and IZ on vertical dense raster SD-OCT scan in both patients, which was more evident on en face EZ map (Figs. 6D, 6E, 6I, 6J). AO cone density map showed moderate cone loss in the parafoveal region, which was more pronounced in the older sibling (Fig. 7A). Quantitative analysis of AO images showed low CD at 2 degrees eccentricity on all meridians in both patients with AFSM and 3 degrees and 4 degrees eccentricities on inferior and superior meridians in the older sibling (2647/II:2), as compared with normal ranges (Fig. 7B, Supplementary Table S4).

Genetic Analysis

Genetic analyses identified 14 different *CRB1* variants in this cohort (Supplementary Fig. S4), including 6 missense variants, 2 in-frame deletions, 2 nonsense variants, 2 splice site/near splice site variants, 1 frameshifting variant, and 1 substitution variant resulting in an in-frame exon deletion.[34] Of these, 11 were reported variants, including 1 hypomorphic variant, and the remaining 3 were novel. Of these, 13 were assessed as likely pathogenic or pathogenic and 1 was a novel variant of uncertain significance (Supplementary Table S5).

Table 2. Baseline Macular Volume Profile in Patients Compared With Age-Matched Healthy Controls

Phenotype	Patient ID	Age (y)	CSV (mm^3)	TMV (mm^3)	IRV (mm^3)	ORV (mm^3)	TMV/ CSV	IRV/ CSV	ORV/ CSV
RP	0058/II:1	47	0.20 **(−1.0)**	11.16[a] **(+9.5)**	0.60[a] **(+2.3)**	2.14[a] **(+9.5)**	55.80[a] **(+5.6)**	3.00[a] **(+3.4)**	10.69[a] **(+5.9)**
	0058/II:2	45	0.16[b] **(−3.0)**	9.50[a] **(+2.7)**	0.53 **(0.0)**	1.78[a] **(+3.5)**	59.37[a] **(+6.9)**	3.28[a] **(+5.3)**	11.09[a] **(+6.7)**
	0432/II:4	48	0.16[b] **(−3.0)**	8.72 **(+0.2)**	0.48 **(−1.7)**	1.67 **(+1.7)**	54.50[a] **(+5.2)**	2.97[a] **(+3.2)**	10.41[a] **(+5.5)**
	0264/II:1	29	0.21 **(0.0)**	9.18[a] **(+2.1)**	0.52 **(−0.5)**	1.72[a] **(+2.8)**	43.71 **(+0.8)**	2.49 **(−0.3)**	8.18 **(+1.2)**
	2118/II:1	11	0.15[b] **(−3.0)**	10.07[a] **(+4.9)**	0.56 **(+1.5)**	1.92[a] **(+6.2)**	67.13[a] **(+7.9)**	3.73[a] **(+5.3)**	12.80[a] **(+8.5)**
MD	0116/II:3	68	0.05[b] **(−8.0)**	5.48[b] **(−8.1)**	0.25[b] **(−13.5)**	1.11[b] **(−5.7)**	109.60[a] **(+20.0)**	4.90[a] **(+11.6)**	22.25[a] **(+23.0)**
	0625/II:1	43	0.12[b] **(−5.0)**	8.45 **(−0.7)**	0.44[b] **(−3.0)**	1.65 **(+1.3)**	70.42[a] **(+10.8)**	3.65[a] **(+7.4)**	13.71[a] **(+11.2)**
	0237/II:2	35	0.17 **(−2.0)**	8.35 **(−0.6)**	0.49 **(−2.0)**	1.56 **(+0.2)**	49.12[a] **(+2.5)**	2.88 **(+1.5)**	9.15[a] **(+2.7)**
	2647/II:3	23	0.13[b] **(−4.0)**	7.87[b] **(−2.2)**	0.45[b] **(−4.0)**	1.40[b] **(−2.5)**	60.54[a] **(+5.9)**	3.46[a] **(+4.1)**	11.44[a] **(+6.3)**
AFSM	2647/II:2	26	0.19 **(−1.0)**	8.55 **(0.0)**	0.52 **(−0.5)**	1.57 **(+0.3)**	45.00 **(+1.2)**	2.75 **(+0.9)**	8.24 **(+1.3)**
	2647/II:4	23	0.21 **(0.0)**	9.02 **(+1.5)**	0.57 **(+2.0)**	1.64 **(+1.5)**	42.95 **(+0.6)**	2.69 **(+0.6)**	7.80 **(+0.6)**

Z-scores are shown in parentheses.

[a]More than 2 SD greater than average of healthy controls.

[b]More than 2 SD smaller than average of healthy controls.

AFSM, asymptomatic fenestrated slit maculopathy; CSV, central subfield volume; IRV, inner ring volume; MD, macular dystrophy; ORV, outer ring volume; RP, retinitis pigmentosa; TMV, total macular volume.

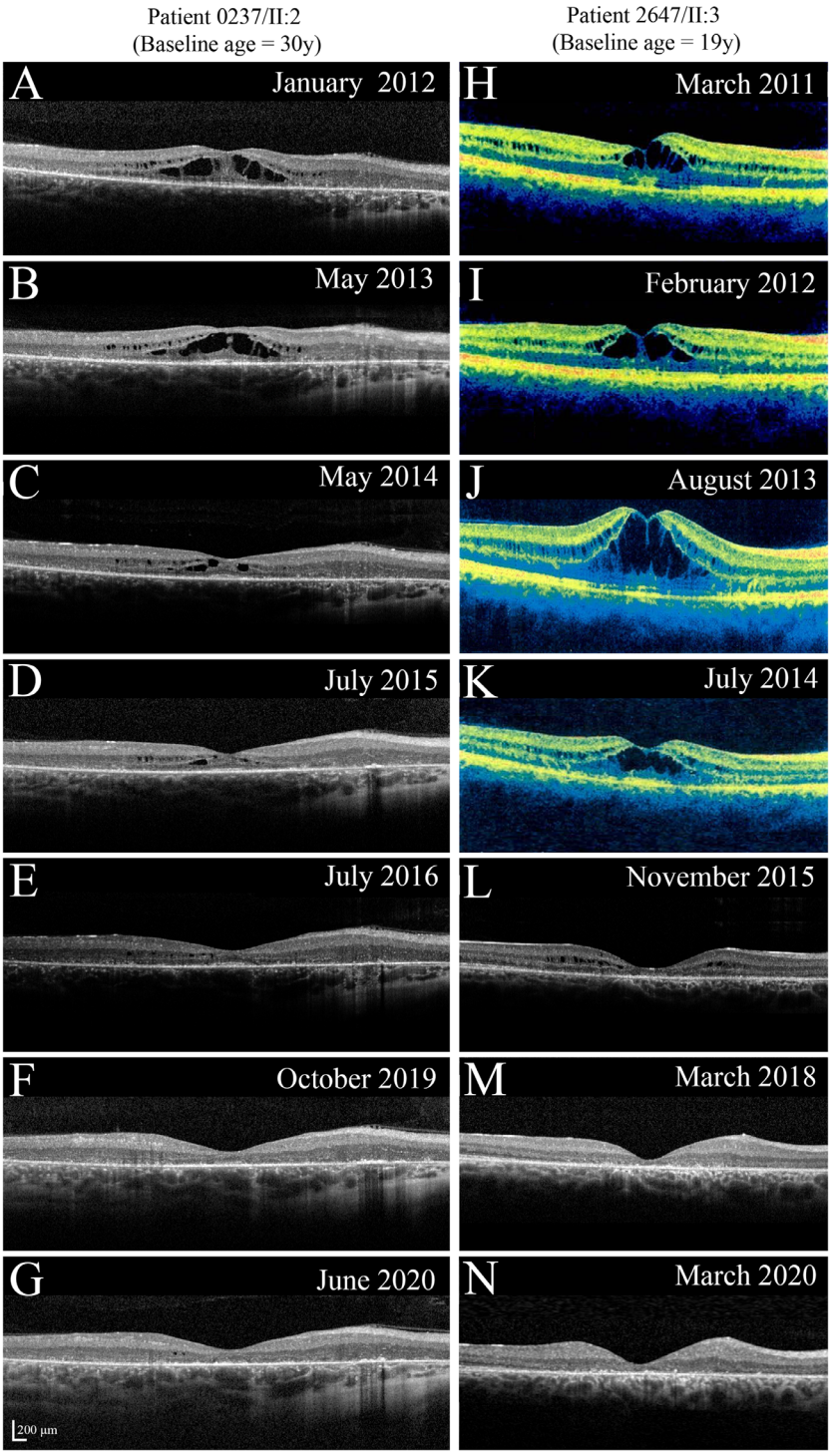

Figure 4. Natural history of cystoid maculopathy in two patients with macular dystrophy. Serial SD-OCT in patient 0237/II:2 (**A–G**) showing severe cystoid maculopathy at baseline **A** and gradual resolution of the intraretinal fluid **B** to **D**, followed by progressive outer retinal atrophy and perifoveal thickening **D** to **G**. Similar pattern was observed in patient 2647/II:3 as documented in retrospective time-domain OCT (**H–K**) and SD-OCT (**L–N**). Serial imaging in both patients revealed progressive attenuation and shortening of the ellipsoid zone (EZ). However, the span of the residual EZ was not measurable due to severe macular edema.

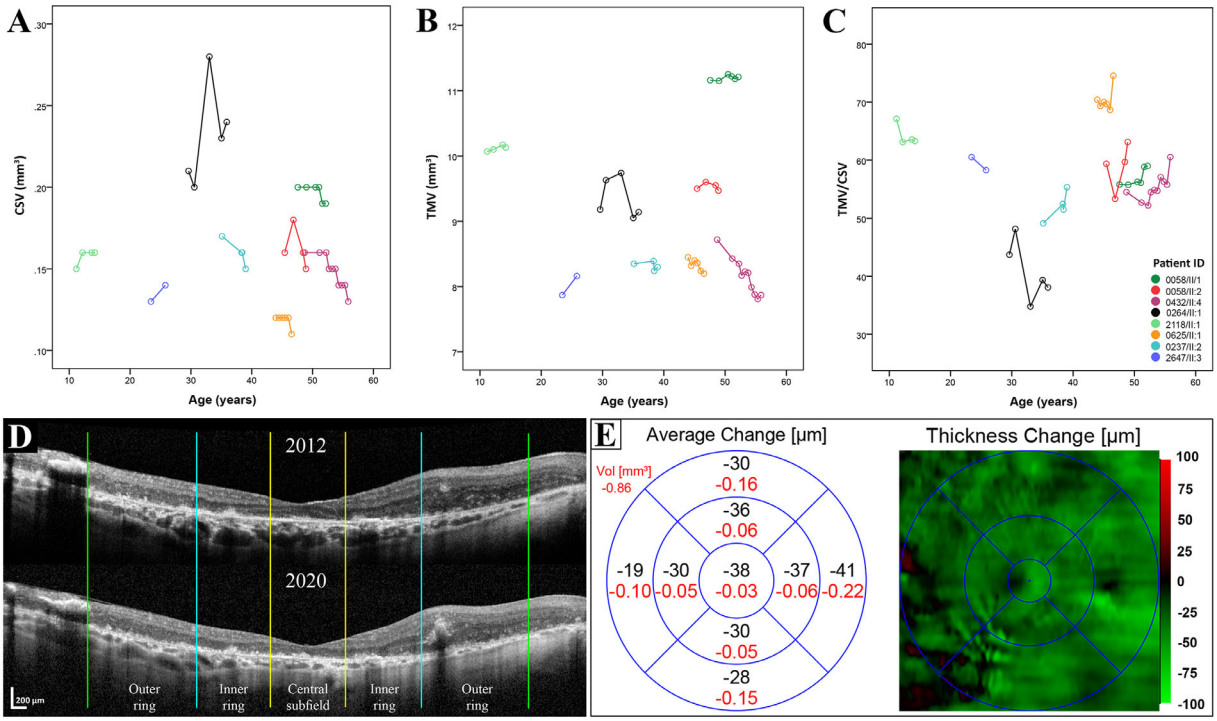

Figure 5. Longitudinal changes in central subfield volume (CSV), total macular volume (TMV) and TMV/CSV ratio in eight patients (5 with retinitis pigmentosa and 3 with macular dystrophy) are shown in panels (**A**, **B**, and **C**), respectively. CSV increased in patients below 30 ($n = 3$) and declined in patients above 30 ($n = 5$) with increasing age **A**. TMV/CSV demonstrated a similar pattern, but in the opposite direction **C**. An example of cross-section B-scan of patient 0432/II:4 at baseline and after 8 years follow up is presented (**D**), beside volume and thickness change map (**E**). Central 1, 3, and 6 mm boundaries on B-scans are marked using *yellow*, *blue*, and *green vertical lines*, respectively. Despite notable decline in CSV (−0.03 mm^3) and TMV (−0.86 mm^3), the ratio of TMV/CSV increased by 6.02 **E**.

Discussion

Pathogenic variants in *CRB1* result in a wide spectrum of inherited retinal diseases ranging from LCA and adult-onset RP to maculopathy.[6,13] Accurate monitoring of disease progression has been hampered by the significant functional and structural damage already present at the time of diagnosis in most patients.[16] Based on widefield FAF, we observed two broad *CRB1* phenotypes: a pan-retinopathy and a maculopathy. We noted that all patients with RP had clearly visible PPRPE on widefield FAF. In both pan-retinopathy and maculopathy groups, we were able to quantify foveal sensitivity and the unique macular volume profile even in advanced stages of the disease. Furthermore, we report compound heterozygous mutations in *CRB1* that resulted in both an MD and a previously undescribed phenotype of AFSM within the same family. We also report three novel mutations, including a splicing variant (c.652+5G>C) in one patient with MD, which is predicted to cause aberrant splicing and is likely pathogenic.

Microperimetry: A Potential Functional End Point in *CRB1*-Retinopathy

Feasibility of microperimetry was previously shown in one patient with advanced *CRB1*-maculopathy using MP1 microperimeter (Nidek Technologies, Padova, Italy).[7] The patient in this study was a 45-year-old woman who carried compound heterozygous *CRB1* mutations, c.[3991C>T];[4142C>T]. Using 10-2 grid, the patient could respond to only 2 parafoveal stimuli in the better eye at baseline, which reduced to 1 stimulus after 5 years.[7] We expand these findings to a larger sample of patients with *CRB1* with varying disease phenotypes and severities and using the two MAIA grid patterns, and report a wide range of residual retinal sensitivities and progression patterns (see Fig. 3). We also demonstrate functional disease progression using both foveal (6 degrees) and macular (10-2) grids, although stable or improving function were also detected. For instance, we observed increasing MS and number of seeing loci in our 11-year-old patient with RP (Figs. 3G, 3H), which may be explained by lower sensitivity and higher variability of

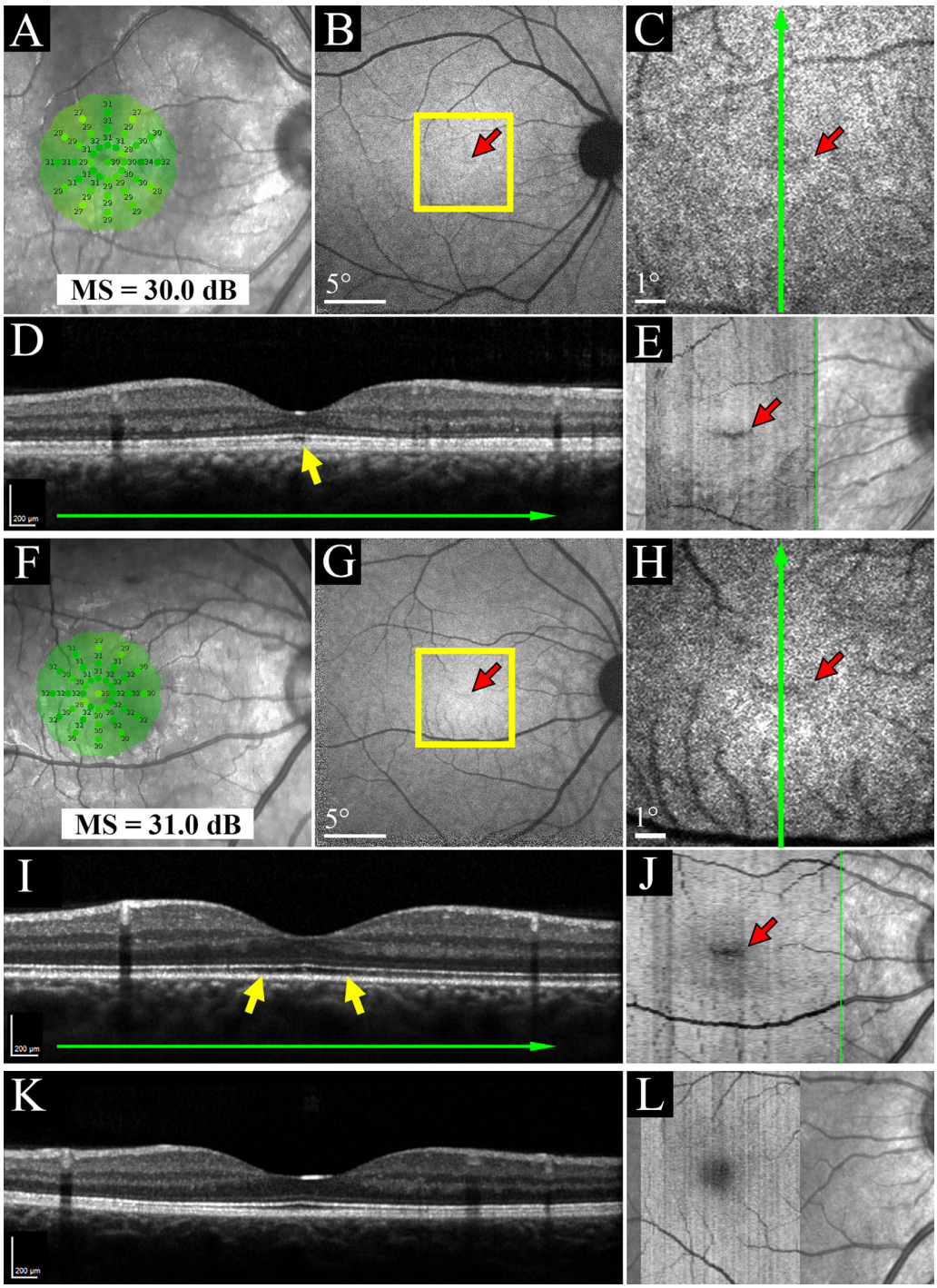

Figure 6. Microperimetry and multimodal imaging in the two patients with asymptomatic fenestrated slit maculopathy (AFSM). Both patients had 20/20 or better visual acuity and normal foveal sensitivity (**A**) and (**F**). Near-infrared autofluorescence (NI-AF) revealed a horizontal slit-like hypo-autofluorescent line (*red arrows*) in both patients (**B**, **C** and **G**, **H**). Vertical dense raster SD-OCT imaging through the hypo-autofluorescent lesion (*green lines* in panels **C** and **H**) demonstrated attenuated ellipsoid zone (EZ) and interdigitating zone (IZ) beneath the fovea (**D** and **I**, *yellow arrows*). Reconstructed en face EZ map highlighted the slit-like EZ defect (*red arrows*) in both patients (**E** and **J**). There is a minor vessel misalignment between EZ en face reconstructions and background infrared image in panel **E**, which is not expected to affect the morphology of the EZ defect. Normal OCT (**K**) and en face EZ map (**L**) using the same protocol in an age-matched healthy control is presented for comparison.

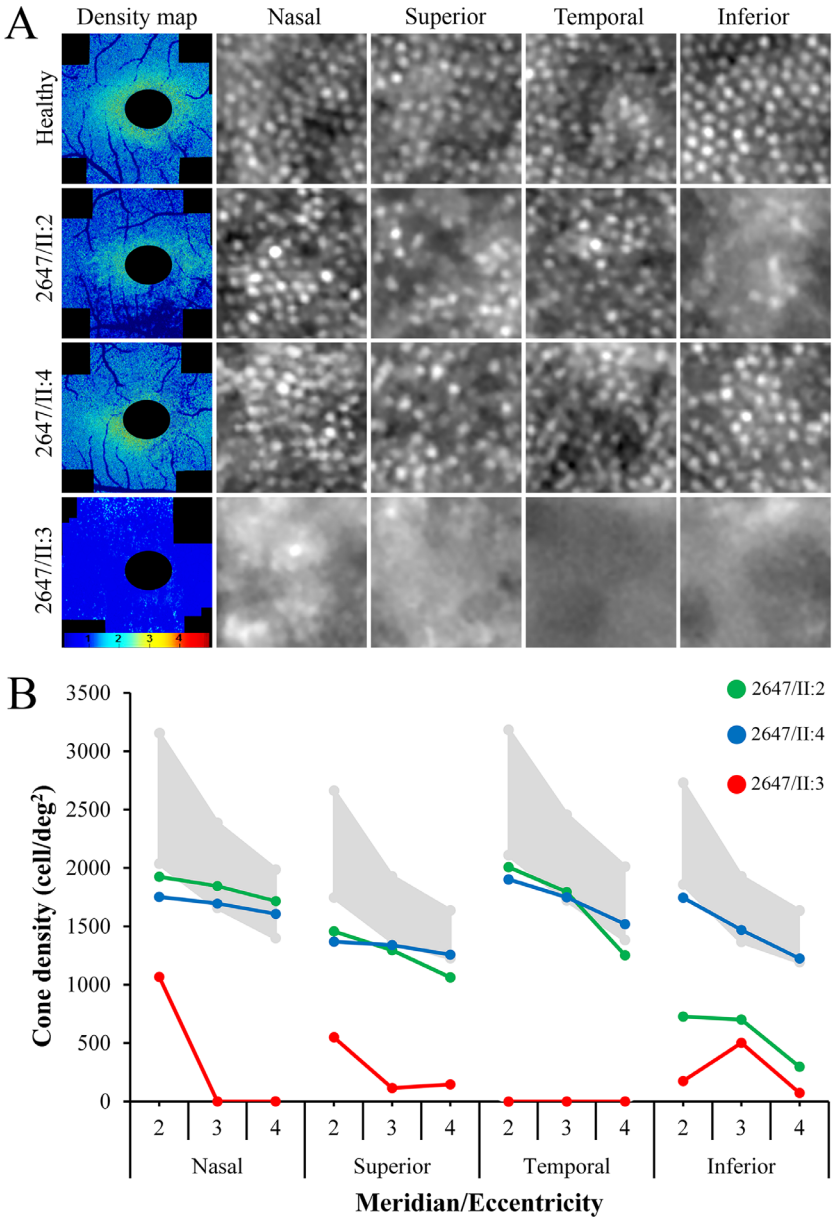

Figure 7. Adaptive optics (AO) imaging findings in three siblings from family 2647 at same age range. Panel (**A**) shows cone density map and examples of cone mosaic imaging at 2 degrees eccentricity in patients with asymptomatic fenestrated slit maculopathy (AFSM) and macular dystrophy (MD) compared with a healthy subject. Density map showed moderate perifoveal cone loss in AFSM (second and third rows) and severe generalized cone loss in MD (*bottom row*). The color code in the bottom row shows cone density ($\times 10^3$ cells/deg^2). Central 2.0 degrees (vertical) - 2.5 degrees (horizontal) is blocked due to lack of resolution to resolve foveal cones. Varying degrees of cone loss was observed in superior and inferior locations in AFSM and all locations in MD. Panel (**B**) shows cone density at 2 degrees, 3 degrees, and 4 degrees eccentricities in four meridional directions. The patient with MD had either no or few visible cones in most locations. Both patients with AFSM had lower cone density at 2 degrees location on all meridians. Additionally, patient II:2 had low cone density at all superior and inferior locations. The grey zone shows ±2 SD of normal CD values reported by Legras et al.[18]

MAIA microperimetry in children.[35] Taken altogether, we suggest that microperimetry should be considered as a feasible method for documenting and monitoring residual retinal function in patients with *CRB1*-retinopathy.

Ultra-Widefield FAF Enhances Visualization of PPRPE in all Patients With *CRB1*-RP

Although PPRPE in RP was described 4 decades ago for the first time,[36] its pathophysiologic

mechanisms and clinical relevance are yet to be explored. It has been proposed that release of a permeable factor from retinal arterioles prevents degeneration of surrounding structures.[36] Whereas PPRPE was initially linked to *CRB1*,[37] genetic analysis may fail to detect a mutation in *CRB1* in up to one third of patients with PPRPE.[37,38] In addition, there are reports of *CRB1*-RP without PPRPE,[39] indicating that PPRPE is neither pathognomonic nor mandatory for diagnosing *CRB1*-RP.

The pan-retinal phenotype demonstrated bilateral PPRPE on ultra-widefield FAF in all our patients with RP. This feature was less prominent on color fundus photographs, particularly in those with less advanced disease. Studies that reported *CRB1*-RP without PPRPE either relied on fundus examination alone[15,39] or included patients with LCA.[14,40] Moreover, no other gene has been linked to RP with PPRPE so far, indicating that a thorough genetic analysis may unveil *CRB1* mutation. Further studies are required to investigate the sensitivity and specificity of PPRPE for *CRB1* mutation. However, given the finding that PPRPE can increase the likelihood of *CRB1* mutations to up to 74%,[3,38] we recommend the use of ultra-widefield FAF imaging in all patients diagnosed with autosomal recessive RP to look for this specific sign.

Perifoveal-to-Foveal Volume Ratio: A Potential Structural End Point in *CRB1*-Retinopathy

Perifoveal retinal thickening has been one of the most consistent findings in *CRB1*-associated retinopathies.[14,15,41] Jacobson and colleagues reported significant perifoveal retinal thickening in eight patients with *CRB1*-LCA/early-onset RP, whereas the retina was thinner compared with normal controls in two patients with RPE65 and one patient with GUCY2D. They used time-domain OCT (Zeiss Humphrey Instruments, Dublin, CA, USA) to measure cross-sectional retinal thickness in a single B-scan.[14] Using time-domain Topcon 3D OCT-1000 (Topcon Medical Systems, Tokyo, Japan), perifoveal retinal thickening was observed in 77% (10/13)[41] and 82% (9/11)[15] of patients with *CRB1*-RP. In addition, increased central subfield retinal thickness (CRT) was noted in 36% (4/11)[15] and 62% (8/13) of patients.[41] Both CRT and perifoveal thickness showed an age-dependent decrease, which was attributed to resolution of macular edema or development of atrophy in the outer retinal layers with increasing age.[41] Unlike all of the aforementioned studies that report time-domain OCT thickness results in LCA/RP, we report for the first time the detailed macular volume profile using the higher resolution SD-OCT in patients with both RP and maculopathy. We also introduce novel OCT parameters, TMV/CSV, and ORV/CSV that are increased in 89% (8/9) of patients with symptomatic *CRB1*-retinopathy. We propose that perifoveal-to-foveal volume ratio highlights relative foveal thinning and perifoveal inner retinal thickening, even if both values are within normal ranges. However, the implications of this marker in genotype-phenotype correlation remain to be explored in larger patient cohorts, including patients with other genetic diagnoses.

Longitudinal analysis of macular volume parameters revealed a biphasic pattern in CSV and TMV/CSV, but not in TMV and ORV. None of our patients had significant macular edema at the time of baseline imaging for the macular volume study and during follow-up phase. Hence, in contrast to previous reports of macular thickness change with increasing age,[41] it is unlikely that our observation was confounded by macular edema. We hypothesize that continued foveal gliosis after initial resolution of CMO may be responsible for increasing CSV until the early to mid-30s. After this phase, progressive foveal thinning results in decreasing CSV and increasing TMV/CSV and ORV/CSV with increasing age. Hence, CSV and TMV/CSV (but not TMV or ORV) might be considered as surrogate structural end points in *CRB1* clinical trials, especially in late-stage disease. However, these speculations need to be investigated in larger populations with longer follow-ups and be correlated with histology.

Asymptomatic Fenestrated Slit Maculopathy: A Novel *CRB1*-Maculopathy Phenotype

We detected the common c.498_506del mutation in 3 out of 4 families. This is an in-frame deletion in exon 2, which was classified as a hypomorphic allele and was reported most frequently in association with *CRB1*-associated maculopathy,[10] as well as in 6 of 43 *CRB1*-associated LCA/RP families, including 1 homozygous and 5 heterozygous.[3] The remaining family (0625) was diagnosed with compound heterozygous mutations, including the novel c.652+5G>C mutation, which is predicted to cause aberrant splicing and is likely pathogenic, and the previously reported c.2843G>A, which is a pathogenic missense mutation.[13] Regardless of causative mutation, the typical natural history of *CRB1*-associated MD comprises childhood or juvenile-onset cystoid maculopathy followed by progressive macular atrophy and vision loss.[7–11]

Cystoid maculopathy can develop at ages as early as 8 years old[10] to as late as mid-40s,[11] and central atrophy can occur between the second[9] and the fifth[11] decades of life. Clinical presentation of our symptomatic cases was comparable to those described in previous reports. In addition, we add long-term natural history of cystoid maculopathy using serial OCT in two patients (see Fig. 4), one of them (0237/II:2) reported as isolated foveal retinoschisis prior to genotyping.[42]

In addition to patients with typical *CRB1*-associated MD, we described 2 asymptomatic cases, who were siblings of a patient with typical MD, carrying biallelic c.498_506del and c.2843G>A variants with only subtle outer retinal changes. This novel AFSM phenotype, which was characterized by AO and microperimetry, has not been previously reported. In a series of 7 cases with the c.498_506del allele, 3 patients (including one homozygous) were asymptomatic at the time of presentation (10–30 years old), however, their visual acuity, OCT, and FAF were grossly abnormal.[10] Conversely, our patients with AFSM displayed normal visual acuity and unremarkable OCT findings in the second decade of life. Long-term follow-up will unveil whether this new phenotype remains structurally stable (i.e. forme fruste state) or a preclinical stage that will evolve into MD as manifested by their sibling with the same variants. The clinical manifestation of AFSM may resemble occult macular dystrophy (OMD), a hereditary macular dystrophy characterized by foveal dysfunction despite normal fundus appearance. The most common genetic abnormality in OMD families has been the *RP1L1* mutation with autosomal dominant inheritance. Furthermore, patients with OMD usually present with reduced visual acuity and central macular dysfunction,[43,44] which are not features found in our AFSM cases.

Limitations

Our study was limited by a lack of ERG data. This would be useful in those patients with asymptomatic maculopathy. A baseline multifocal and pattern ERG could be helpful for detecting subclinical functional abnormalities in patients with normal visual acuity and foveal sensitivity. In addition, we have not provided long-term data for the novel AFSM phenotype described.

Conclusions

We showed that PPRPE is best visualized with ultra-widefield FAF imaging in patients with *CRB1*-RP. Microperimetry may be useful in monitoring foveal function in moderate macular dystrophy cases given our observation of preserved foveal sensitivity. We found the macular volume profile, especially the ratio of perifoveal-to-foveal retinal volume, may be used as a surrogate structural outcome measure in both pan-retinopathy and maculopathy phenotypes even in the advanced cases. AFSM may represent a forme fruste state or preclinical stage of *CRB1*-associated MD. Longer term studies are required to validate the utility of microperimetry and macular volume profile in measuring disease progression rate. Recognition of AFSM phenotype provides an opportunity for examining disease modifying genes or early intervention to prevent cystoid maculopathy.

Acknowledgments

The authors thank Amanda Scurry and Jayme Glynn for their assistance in organizing the patient appointments for the clinical assessments. The AIRDR acknowledges the assistance of Ling Hoffman and Isabella Urwin from the Department of Medical Technology and Physics at Sir Charles Gairdner Hospital.

Supported by the Australian National Health and Medical Research Council under GNT116360 (to F.K.C.), GNT1188694 (to F.K.C.), GNT1054712 (to F.K.C.), and MRF1142962 (to F.K.C.), McCusker Foundation (to F.K.C.), Miocevich Retina Fellowship (to R.H.J.), Retina Australia (to J.A.T., T.L., J.N.D.R., and T.L.M.) and the UWA Postgraduate Research Scholarship (to D.R.). The sponsor or funding organization had no role in the design or conduct of this research.

Disclosure: **D. Roshandel,** None; **J.A. Thompson,** None; **R.C. Heath Jeffery,** None; **D.M. Sampson,** None; **E. Chelva,** None; **T.L. McLaren,** None; **T.M. Lamey,** None; **J.N. De Roach,** None; **S.R. Durkin,** None; **F.K. Chen,** None

References

1. Gosens I, den Hollander AI, Cremers FP, Roepman R. Composition and function of the Crumbs protein complex in the mammalian retina. *Exp Eye Res.* 2008;86:713–726.
2. Mehalow AK, Kameya S, Smith RS, et al. CRB1 is essential for external limiting membrane integrity and photoreceptor morphogenesis in the

mammalian retina. *Hum Mol Genet.* 2003;12: 2179–2189.
3. Corton M, Tatu SD, Avila-Fernandez A, et al. High frequency of CRB1 mutations as cause of early-onset retinal dystrophies in the Spanish population. *Orphanet J Rare Dis.* 2013;8:20.
4. Ehrenberg M, Pierce EA, Cox GF, Fulton AB. CRB1: one gene, many phenotypes. *Semin Ophthalmol.* 2013;28:397–405.
5. Thompson JA, De Roach JN, McLaren TL, et al. The genetic profile of Leber congenital amaurosis in an Australian cohort. *Mol Genet Genomic Med.* 2017;5:652–667.
6. Vincent A, Ng J, Gerth-Kahlert C, et al. Biallelic mutations in CRB1 underlie autosomal recessive familial foveal retinoschisis. *Invest Ophthalmol Vis Sci.* 2016;57:2637–2646.
7. Tsang SH, Burke T, Oll M, et al. Whole exome sequencing identifies CRB1 defect in an unusual maculopathy phenotype. *Ophthalmology.* 2014;121:1773–1782.
8. Wolfson Y, Applegate CD, Strauss RW, Han IC, Scholl HP. CRB1-related maculopathy with cystoid macular edema. *JAMA Ophthalmol.* 2015;133:1357–1360.
9. Shah N, Damani MR, Zhu XS, et al. Isolated maculopathy associated with biallelic CRB1 mutations. *Ophthalmic Genet.* 2017;38:190–193.
10. Khan KN, Robson A, Mahroo OAR, et al. A clinical and molecular characterisation of CRB1-associated maculopathy. *Eur J Hum Genet.* 2018;26:687–694.
11. Mucciolo DP, Murro V, Giorgio D, et al. Long-term follow-up of a CRB1-associated maculopathy. *Ophthalmic Genetics.* 2018;39:522–525.
12. Pellissier LP, Quinn PM, Alves CH, et al. Gene therapy into photoreceptors and Muller glial cells restores retinal structure and function in CRB1 retinitis pigmentosa mouse models. *Hum Mol Genet.* 2015;24:3104–3118.
13. Bujakowska K, Audo I, Mohand-Said S, et al. CRB1 mutations in inherited retinal dystrophies. *Hum Mutat.* 2012;33:306–315.
14. Jacobson SG, Cideciyan AV, Aleman TS, et al. Crumbs homolog 1 (CRB1) mutations result in a thick human retina with abnormal lamination. *Hum Mol Genet.* 2003;12:1073–1078.
15. Talib M, van Schooneveld MJ, van Genderen MM, et al. Genotypic and phenotypic characteristics of CRB1-associated retinal dystrophies: a long-term follow-up study. *Ophthalmology.* 2017;124:884–895.
16. Stingl KT, Kuehlewein L, Weisschuh N, et al. Chromatic full-field stimulus threshold and pupillography as functional markers for late-stage, early-onset retinitis pigmentosa caused by CRB1 mutations. *Transl Vis Sci Technol.* 2019;8:45.
17. McCulloch DL, Marmor MF, Brigell MG, et al. ISCEV Standard for full-field clinical electroretinography (2015 update). *Doc Ophthalmol.* 2015;130:1–12.
18. Legras R, Gaudric A, Woog K. Distribution of cone density, spacing and arrangement in adult healthy retinas with adaptive optics flood illumination. *PLoS One.* 2018;13:e0191141.
19. Bukowska DM, Chew AL, Huynh E, et al. Semi-automated identification of cones in the human retina using circle Hough transform. *Biomed Opt Express.* 2015;6:4676–4693.
20. De Roach JN, McLaren TL, Paterson RL, et al. Establishment and evolution of the Australian Inherited Retinal Disease Register and DNA Bank. *Clin Exp Ophthalmol.* 2013;41:476–483.
21. Chiang JP, Lamey T, McLaren T, Thompson JA, Montgomery H, De Roach J. Progress and prospects of next-generation sequencing testing for inherited retinal dystrophy. *Expert Rev Mol Diagn.* 2015;15:1269–1275.
22. den Dunnen JT, Dalgleish R, Maglott DR, et al. HGVS Recommendations for the Description of Sequence Variants: 2016 Update. *Hum Mutat.* 2016;37:564–569.
23. Jagadeesh KA, Wenger AM, Berger MJ, et al. M-CAP eliminates a majority of variants of uncertain significance in clinical exomes at high sensitivity. *Nat Genet.* 2016;48:1581–1586.
24. Ioannidis NM, Rothstein JH, Pejaver V, et al. REVEL: an ensemble method for predicting the pathogenicity of rare missense variants. *Am J Hum Genet.* 2016;99:877–885.
25. Schwarz JM, Rodelsperger C, Schuelke M, Seelow D. MutationTaster evaluates disease-causing potential of sequence alterations. *Nat Meth.* 2010;7:575–576.
26. Adzhubei IA, Schmidt S, Peshkin L, et al. A method and server for predicting damaging missense mutations. *Nat Methods.* 2010;7:248–249.
27. Ng PC, Henikoff S. Predicting deleterious amino acid substitutions. *Genome Res.* 2001;11:863–874.
28. Douville C, Masica DL, Stenson PD, et al. Assessing the pathogenicity of insertion and deletion variants with the variant effect scoring tool (VEST-Indel). *Hum Mutat.* 2016;37:28–35.
29. Stenson PD, Mort M, Ball EV, et al. The Human Gene Mutation Database: towards a comprehensive repository of inherited mutation data for medical research, genetic diagnosis and next-generation sequencing studies. *Hum Genet.* 2017;136:665–677.

30. Karczewski KJ, Francioli LC, Tiao G, et al. Variation across 141,456 human exomes and genomes reveals the spectrum of loss-of-function intolerance across human protein-coding genes. *BioRxiv*, https://doi.org/10.1101/531210.
31. Richards S, Aziz N, Bale S, et al. Standards and guidelines for the interpretation of sequence variants: a joint consensus recommendation of the American College of Medical Genetics and Genomics and the Association for Molecular Pathology. *Genet Med.* 2015;17:405–424.
32. Jarvik GP, Browning BL. Consideration of cosegregation in the pathogenicity classification of genomic variants. *Am J Hum Genet.* 2016;98:1077–1081.
33. Abou Tayoun AN, Pesaran T, DiStefano MT, et al. Recommendations for interpreting the loss of function PVS1 ACMG/AMP variant criterion. *Hum Mutat.* 2018;39:1517–1524.
34. Zhang X, Thompson JA, Zhang D, et al. Characterization of CRB1 splicing in retinal organoids derived from a patient with adult-onset rod-cone dystrophy caused by the c.1892A>G and c.2548G>A variants. *Mol Genet Genomic Med.* 2020;8(11):e1489.
35. Jones PR, Yasoubi N, Nardini M, Rubin GS. Feasibility of macular integrity assessment (MAIA) microperimetry in children: sensitivity, reliability, and fixation stability in healthy observers. *Invest Ophthalmol Vis Sci.* 2016;57:6349–6359.
36. Heckenlively JR. Preserved para-arteriole retinal pigment epithelium (PPRPE) in retinitis pigmentosa. *Br J Ophthalmol.* 1982;66:26–30.
37. den Hollander AI, ten Brink JB, de Kok YJ, et al. Mutations in a human homologue of Drosophila crumbs cause retinitis pigmentosa (RP12). *Nat Genet.* 1999;23:217–221.
38. den Hollander AI, Davis J, van der Velde-Visser SD, et al. CRB1 mutation spectrum in inherited retinal dystrophies. *Hum Mutat.* 2004;24:355–369.
39. Lotery AJ, Malik A, Shami SA, et al. CRB1 mutations may result in retinitis pigmentosa without para-arteriolar RPE preservation. *Ophthalmic Genet.* 2001;22:163–169.
40. Henderson RH, Mackay DS, Li Z, et al. Phenotypic variability in patients with retinal dystrophies due to mutations in CRB1. *Br J Ophthalmol.* 2011;95:811–817.
41. Mathijssen IB, Florijn RJ, Van den Born LI, et al. Long-term follow-up of patients with retinitis pigmentosa type 12 caused by CRB1 mutations. *Retina.* 2017;37:161–172.
42. Chen FK, McAllister IL, Chelva ES. Thirteen-year follow up of isolated foveal retinoschisis in a 24-year-old woman. *Clin Exp Ophthalmol.* 2006;34:600–605.
43. Miyake Y, Horiguchi M, Tomita N, et al. Occult macular dystrophy. *Am J Ophthalmol.* 1996;122:644–653.
44. Fujinami K, Yang L, Joo K, et al. Clinical and genetic characteristics of East Asian patients with occult macular dystrophy (Miyake Disease): East Asia Occult Macular Dystrophy Studies Report Number 1. *Ophthalmology.* 2019;126:1432–1444.